Letter Vol. 44, No. 15 / 1 August 2019 / Optics Letters 3613

Optics Letters

Generation of Gaussian-modulated entangled states for continuous variable quantum communication

Ning Wang,[1] Shanna Du,[1] Wenyuan Liu,[1] Xuyang Wang,[1,2] and Yongmin Li[1,2,*]

[1]State Key Laboratory of Quantum Optics and Quantum Optics Devices, Institute of Opto-Electronics, Shanxi University, Taiyuan 030006, China
[2]Collaborative Innovation Center of Extreme Optics, Shanxi University, Taiyuan 030006, China
*Corresponding author: yongmin@sxu.edu.cn

Received 27 May 2019; revised 17 June 2019; accepted 17 June 2019; posted 19 June 2019 (Doc. ID 368457); published 17 July 2019

We present and demonstrate a high-efficiency and compact scheme for generating Gaussian-modulated Einstein–Podolsky–Rosen (EPR) entangled optical fields by injecting a modulated signal field into a non-degenerate optical parametric amplifier (NOPA). We perform a quantum analysis of the scheme and derive the variance of the output signal (idler) mode and the quantum entanglement between the signal and idler modes from the NOPA. An experimental study is presented with different Gaussian modulation depths, showing that the modulation of the injected signal field successfully enlarges the distribution of the field quadratures of the EPR source in phase space and has a negligible effect on the entanglement quality. The experimental observations have good agreement with the theoretical analysis. Our scheme can be used readily in continuous variable quantum key distribution protocol.

https://doi.org/10.1364/OL.44.003613

Quantum key distribution (QKD) promises the information theoretical security of the sharing key between legitimate parties, when combined with one-time-pad encryption, providing a powerful solution to the issues of secure communication. QKD encodes key information on the quantum state, and its security relies on the fundamental laws of quantum mechanics; thus, any eavesdropping, in principle, can be detected. Since the invention of the first QKD protocol, the BB84 protocol, great progress has been made on both the theoretical and experimental fronts, and the various field tests have also been implemented [1,2]. The continuous variable (CV) QKD technique [3–9] can exploit standard telecommunication technology and has a high secret key rate at the metropolitan area due to the encoding on the multi-photon and high-dimensional quantum state.

In conventional coherent-state CV-QKD, the excess noise level severely limits the performance of the system [10]. Recently, it has been shown that the modulated entangled-state protocol can significantly enhance the system's robustness to the excess noise and, hence, improve the transmission distance and secret rate [11,12]. To realize this protocol, the preparation of Gaussian-modulated Einstein–Podolsky–Rosen (EPR) entangled states is an essential prerequisite. The straightforward way of modulating the states is to modulate one beam of the EPR state directly using an amplitude modulator (AM) and a phase modulator (PM). However, this approach will inevitably deteriorate the entanglement characteristics of the EPR states due to the inserted loss of the modulator, which can be over 4 dB for typical waveguide electro-optic modulators currently widely used in the high-speed optical communication field. To overcome this limit, one can alternatively interfere one beam of the entangled fields with an auxiliary modulated beam at a highly non-symmetrical beam splitter [12]. In this case, the entanglement quality remains almost intact at the expense of a complex phase-locking technique and extra equipment.

In this Letter, we present the use of a signal-field-injected non-degenerate optical parametric amplifier (NOPA) to prepare the Gaussian-modulated EPR entangled states, in which the modulation signals are directly applied to the injected signal field. Compared with previous works, our scheme does not require ancilla beams and sophisticated equipment for phase locking; moreover, the inserted losses are eliminated essentially.

The schematic of our scheme is depicted in Fig. 1. The NOPA system consists of three cavity modes that interact

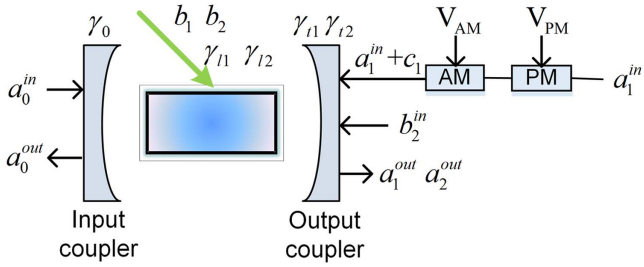

Fig. 1. Conceptual diagram of Gaussian-modulated entangled states protocol. a_0, a_1 (a_2), and b are the pump, signal (idler), and vacuum fields, respectively. c_1 denotes the modulation signal. γ_0, $\gamma_{t1}+\gamma_{l1}$, and $\gamma_{t2}+\gamma_{l2}$ represent the dissipation rates of the cavity modes, i.e., the pump, signal, and idler fields, respectively. Subscript t (l) denotes the dissipation arising from the output coupler (intracavity losses).

inside the nonlinear media, pump mode a_0, signal mode a_1, and idler mode a_1 with angular frequencies of ω_0, ω_1, and ω_2, respectively. We assume that the pump field a_0^{in} is a strong coherent field, and a weak signal field a_1^{in} with Gaussian modulation c_1 is injected into the NOPA. Without loss of generality, the pump field a_0^{in} is treated as real, and the injected signal field has a relative phase shift φ so that $a_1^{\text{in}} = |a_1^{\text{in}}|e^{i\varphi}$. Assuming all three fields are resonant with the cavity, the corresponding quantum Langevin equations can be written as

$$\begin{aligned} da_0/dt &= -\gamma_0 a_0 - \chi a_1 a_2 + \sqrt{2\gamma_0}a_0^{\text{in}}, \\ da_1/dt &= -\gamma_1 a_1 + \chi a_0 a_2^{\dagger} + \sqrt{2\gamma_{t1}}(a_1^{\text{in}} + c_1) + \sqrt{2\gamma_{l1}}b_1, \\ da_2/dt &= -\gamma_2 a_2 + \chi a_0 a_1^{\dagger} + \sqrt{2\gamma_{t2}}b_2^{\text{in}} + \sqrt{2\gamma_{l2}}b_2, \end{aligned} \tag{1}$$

where $\gamma_j = \gamma_{tj} + \gamma_{lj} (j = 0, 1, 2)$ represent the dissipation rates of the cavity modes, and subscript t (l) denotes the dissipation arising from the output coupler (intracavity losses); χ denotes the nonlinear coupling constant; $a_1^{\text{in}}(b_2^{\text{in}})$ represents the input mode of the signal (idler, vacuum state hereafter); b_1 (b_2) represents the intracavity loss of the signal (idler) mode; and c_1 is the classical modulation signal.

We introduce the fluctuation quadrature operators for the pump, signal, and idler modes as

$$\delta X_j = (e^{-i\theta_j}\delta a_j + e^{i\theta_j}\delta a_j^{\dagger}), \qquad \delta Y_j = i(e^{i\theta_j}\delta a_j^{\dagger} - e^{-i\theta_j}\delta a_j), \tag{2}$$

where $\theta_0 = 0$, $\theta_1 = \varphi$ and $\theta_2 = -\varphi$. δX_j and δY_j are the fluctuation of the amplitude and phase quadrature, respectively. With standard linearization and applying Fourier transformation to Eq. (1), the linearized quantum Langevin equations for the fluctuation quadrature operators can be obtained:

$$\begin{aligned} \delta X_1(\Omega) = &-\left\{\begin{array}{l}(\gamma_2+i\Omega)\left[\sqrt{2\gamma_{t1}}(\delta X_{c1}+\delta X_{a1^{\text{in}}})+\sqrt{2\gamma_{l1}}\delta X_{b1}\right] \\ +\chi\alpha_0\left(\sqrt{2\gamma_{t2}}\delta X_{b2^{\text{in}}}+\sqrt{2\gamma_{l2}}\delta X_{b2}\right)\end{array}\right\} \\ &\times[\alpha_0^2\chi^2-(\gamma_1+i\Omega)(\gamma_2+i\Omega)]^{-1}, \\ \delta Y_1(\Omega) = &-\left\{\begin{array}{l}(\gamma_2+i\Omega)\left[\sqrt{2\gamma_{t1}}(\delta Y_{c1}+\delta Y_{a1^{\text{in}}})+\sqrt{2\gamma_{l1}}\delta Y_{b1}\right] \\ -\chi\alpha_0\left(\sqrt{2\gamma_{t2}}\delta Y_{b2^{\text{in}}}+\sqrt{2\gamma_{l2}}\delta Y_{b2}\right)\end{array}\right\} \\ &\times[\alpha_0^2\chi^2-(\gamma_1+i\Omega)(\gamma_2+i\Omega)]^{-1}, \\ \delta X_2(\Omega) = &-\left\{\begin{array}{l}(\gamma_1+i\Omega)\left(\sqrt{2\gamma_{t2}}\delta X_{b2^{\text{in}}}+\sqrt{2\gamma_{l2}}\delta X_{b2}\right) \\ +\chi\alpha_0\left[\sqrt{2\gamma_{t1}}(\delta X_{c1}+\delta X_{a1^{\text{in}}})+\sqrt{2\gamma_{l1}}\delta X_{b1}\right]\end{array}\right\} \\ &\times[\alpha_0^2\chi^2-(\gamma_1+i\Omega)(\gamma_2+i\Omega)]^{-1}, \\ \delta Y_2(\Omega) = &-\left\{\begin{array}{l}(\gamma_2+i\Omega)(\sqrt{2\gamma_{t2}}\delta Y_{b2^{\text{in}}}+\sqrt{2\gamma_{l2}}\delta Y_{b2})- \\ \chi\alpha_0[\sqrt{2\gamma_{t1}}(\delta Y_{c1}+\delta Y_{a1^{\text{in}}})+\sqrt{2\gamma_{l1}}\delta Y_{b1}]\end{array}\right\} \\ &\times[\alpha_0^2\chi^2-(\gamma_1+i\Omega)(\gamma_2+i\Omega)]^{-1}. \end{aligned} \tag{3}$$

To derive Eq. (3), the strong pump is treated as a perfect monochromatic field with a constant amplitude.

To make a comparison between theoretical predictions and experimental observations, the fluctuation field operators outputted from the cavity should be calculated. We assume that the seed field is injected from the output coupler of the NOPA. In this case, using the input-output relations, the output fields are given by

$$\begin{aligned} \delta X_1^{\text{out}}(Y_1^{\text{out}})(\Omega) &= \sqrt{2\gamma_{t1}}\delta X_1(Y_1)(\Omega) - \delta X_{c1}(Y_{c1})(\Omega) \\ &\quad + \delta X_{b1}(Y_{b1})(\Omega), \\ \delta X_2^{\text{out}}(Y_2^{\text{out}})(\Omega) &= \sqrt{2\gamma_{t2}}\delta X_2(Y_2)(\Omega) - \delta X_{b2}(Y_{b2})(\Omega). \end{aligned} \tag{4}$$

The noise power spectrum of the output field quadratures is defined as

$$V_{X_j^{\text{out}}(Y_j^{\text{out}})}(\Omega) = \langle \delta X_j^{\text{out}}(Y_j^{\text{out}})(\Omega)\delta X_j^{\text{out}}(Y_j^{\text{out}})(-\Omega)\rangle. \tag{5}$$

Taking the detection efficiency of the system into account, the measured variance of the amplitude (phase) quadrature of the output fields can be expressed as

$$V_{X_j}^{\text{out}}(V_{Y_j}^{\text{out}})(\Omega) = \eta_j V_{X_j^{\text{out}}(Y_j^{\text{out}})}(\Omega) + 1 - \eta_j, \tag{6}$$

where $\eta_j = \eta_{j,\text{t}} \times \eta_{j,\text{vis}} \times \eta_{j,pd} \times \eta_{j,e}$, η_t is the propagation efficiency, η_{vis} is the interference efficiency, η_{pd} is the quantum efficiency of the photodiodes, and η_e denotes the equivalent efficiency induced by the electronic noises of the measurement apparatus.

To characterize the quantum entanglement, we define two combined field quadratures of the signal and idler modes or, more precisely, the quantum correlations of the amplitude quadrature difference δX_-^{out} and the phase quadrature sum δY_+^{out}:

$$\begin{aligned} \delta X_-^{\text{out}}(\Omega) &= (\delta X_1^{\text{out}}(\Omega) - \delta X_2^{\text{out}}(\Omega))/\sqrt{2}, \\ \delta Y_+^{\text{out}}(\Omega) &= (\delta Y_1^{\text{out}}(\Omega) + \delta Y_2^{\text{out}}(\Omega))/\sqrt{2}. \end{aligned} \tag{7}$$

The corresponding quantum correlation spectra of the combined field quadratures are expressed as

$$\begin{aligned} V_{X_-^{\text{out}}}(\Omega) &= \eta_1\gamma_{t1}V_{X_1}^{\text{out}}(\Omega) + \eta_2\gamma_{t2}V_{X_2}^{\text{out}}(\Omega) + 1 + \frac{V_{\text{AM}}}{2}\eta_1 \\ &\quad - \sqrt{\eta_1\eta_2\gamma_{t1}\gamma_{t2}}(\langle\delta X_1(\Omega)\delta X_2(-\Omega)\rangle \\ &\quad + \langle\delta X_2(\Omega)\delta X_1(-\Omega)\rangle), \\ V_{Y_+^{\text{out}}}(\Omega) &= \eta_1\gamma_{t1}V_{Y_1}^{\text{out}}(\Omega) + \eta_2\gamma_{t2}V_{Y_2}^{\text{out}}(\Omega) + 1 + \frac{V_{\text{PM}}}{2}\eta_1 \\ &\quad + \sqrt{\eta_1\eta_2\gamma_{t1}\gamma_{t2}}(\langle\delta Y_1(\Omega)\delta Y_2(-\Omega)\rangle \\ &\quad + \langle\delta Y_2(\Omega)\delta Y_1(-\Omega)\rangle). \end{aligned} \tag{8}$$

To derive the variance of the output fields, the quantum correlation spectrum of the input field quadratures that characterize the input modulation signal, the input signal (idler) field, and the vacuum fields induced by the intracavity losses are required and given by

$$\begin{aligned} V_{X_{c1}}(\Omega) &= V_{\text{AM}}, \qquad V_{Y_{c1}}(\Omega) = V_{\text{PM}}, \\ V_{X,a1^{\text{in}}}(\Omega) &= V_{Y,b2^{\text{in}}}(\Omega) = 1. \end{aligned} \tag{9}$$

In our experiment, the entanglement of the signal and idler optical fields is quantified in terms of the EPR criterion [13,14], which is a sufficient condition to discriminate quantum entanglement and can be related to the levels of quantum correlations. The EPR criterion is described by the product of conditional variances of the conjugate quadratures (X, Y) between the two optical fields:

$$V_{2|1}^X V_{2|1}^Y < 1, \tag{10}$$

where $V_{2|1}^O = V_2^O - |\langle\delta O_2\delta O_1\rangle|^2/V_1^O$ and $O = (X, Y)$.

The experimental setup for generating the Gaussian-modulated entangled states is shown in Fig. 2. A single-frequency

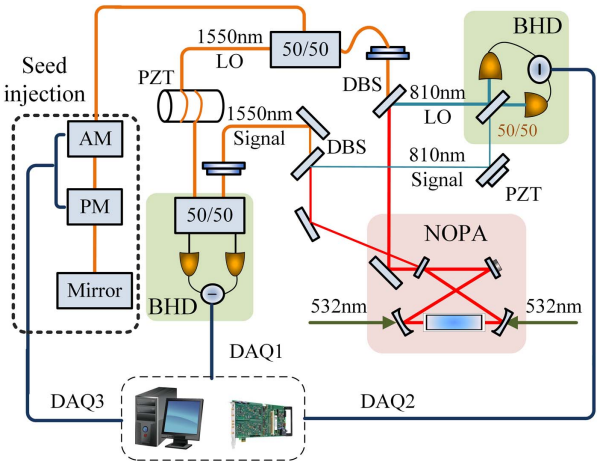

Fig. 2. Schematic of the experimental setup. NOPA, non-degenerate optical parametric amplifier; DBS, dichroic beam splitter; PZT, piezoelectric transducer; LO, local oscillator; PM, phase modulator; AM, amplitude modulator; BHD, balanced homodyne detection; and DAQ, data-acquisition card.

532 nm laser pumps a ring nonlinear resonator from opposite directions [15]. The two-color downconverted fields (1550 nm signal, 810 nm idler) generated above (below) the threshold direction serve as the local oscillator (LO) (signal). The output fields from the NOPA are separated by two dichroic beam splitters, and the resulting 810 nm idler and its LO are detected by a free-space balanced homodyne detector (BHD). The 1550 nm signal and its LO are coupled into a single-mode polarization-maintaining fiber pigtailed 50:50 beam splitter for homodyne detection, which are anti-reflection-coated at 1550 nm to minimize the Fresnel reflection. One portion of the 1550 nm LO is split and modulated by an AM and a PM, which are driven by two independent white noises at a sideband frequency of 3.5 MHz with a bandwidth of 500 kHz. The sideband white noises are generated digitally by mixing 500 kHz bandwidth white noises with a 3.5 MHz carrier signal and the outputs from a two-channel data-acquisition card (DAQ). The modulated beam is then injected into the NOPA to act as the modulated seed field. The temporal width of each quantum state is 2 μs, which is determined by the modulation rate of the white noises.

The amplitude (phase) quadratures of the signal and idler fields are simultaneously detected using their BHDs by setting the relative phases between the quantum fields and the corresponding LO at 0 ($\pi/2$). The measured two-output electronic signals are mixed with the 3.5 MHz carrier and filtered using a low-pass filter with a bandwidth of 500 kHz. The resulting filtered signals are sampled using a two-channel DAQ with sampling rates of 10 MHz/s. For each quantum state, 20 data points are sampled, which are summed to obtain the quadratures of each quantum state. To keep the measured quadratures and the modulation signals in phase and synchronized, a radio-frequency power splitter splits the 3.5 MHz carrier signal into four identical output carriers, of which two are employed for the signal modulation, and the rest are used to demodulate the homodyne signals; meanwhile, all three DAQs share one clock signal.

Figure 4 shows the observed experimental data of the amplitude and phase quadratures of the Gaussian-modulated

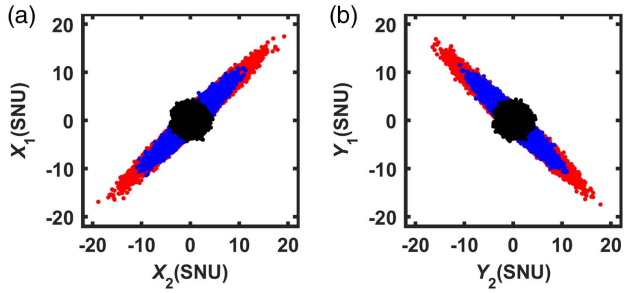

Fig. 3. Observed quadrature correlations. (a) Amplitude quadratures. (b) Phase quadratures. The black points represent the correlations of vacuum states. The blue and red points represent the quadrature correlations of original and Gaussian-modulated EPR states, respectively. The quadrature data are normalized to SNUs.

EPR states. To plot Figs. 4(a) and 4(b), 200,000 quadrature pairs are used, and the measured quadratures have been normalized to shot noise units (SNUs). It can be seen that positive correlations between the amplitude quadratures of the EPR beams exist, whereas negative correlations appear between the phase quadratures, which is consistent with the features of the EPR states generated from a NOPA. It is clear that the Gaussian modulation of the injected seed field significantly enlarges the variances of the quadratures for each EPR beam, which confirms the validity of our scheme.

To gain insight into the entanglement characteristics of the Gaussian-modulated EPR states in Fig. 3, we list the relevant parameters of the EPR source in Table 1. Here (X, Y) and (X_j^M, Y_j^M) denote the quadratures of EPR states without and with the Gaussian modulation, respectively, and V_1 and V_2 are the variances of the quadratures for the signal and idler fields, respectively. $C_{21} = \langle \delta O_2 \delta O_1 \rangle / \sqrt{V_1^O V_2^O}$, $O = (X, Y)$ denote the quantum correlation coefficients; $V_{2|1}$ are the conditional variances of the field quadratures; and V_{sq} denotes two-mode squeezing between the signal and idler fields, which is given by

$$V_{sq} = 10 \log_{10}\left(V_2/2 + V_1/2 - |C_{21}|\sqrt{V_2 V_1}\right). \quad (11)$$

When no modulation exists, each of the output signal and idler fields from the NOPA has a quadrature variance of ~8 SNUs; in addition, they are two-mode squeezed with a squeezing level of 4.9 dB. The inferred product of conditional variances of the conjugate quadratures is $V_{2|1}^X V_{2|1}^Y = 0.44$, which satisfies the EPR criterion defined in Eq. (10) and indicates the existence of the quadrature entanglement. When the signal modulation is switched on, the quadrature variances increase to approximately 19 SNUs. The two-mode squeezing is reduced to 4.3 dB, and

Table 1. Parameters of the EPR Source With and Without Modulation

	V_2	V_1	C_{21}	V_{sq}	$V_{2\|1}$
X	7.7	8.4	0.96	−4.9	0.67
Y	7.5	8.2	−0.96	−4.9	0.66
X^M	18.4	18.7	0.98	−4.3	0.74
Y^M	19.3	19.3	−0.98	−4.4	0.73

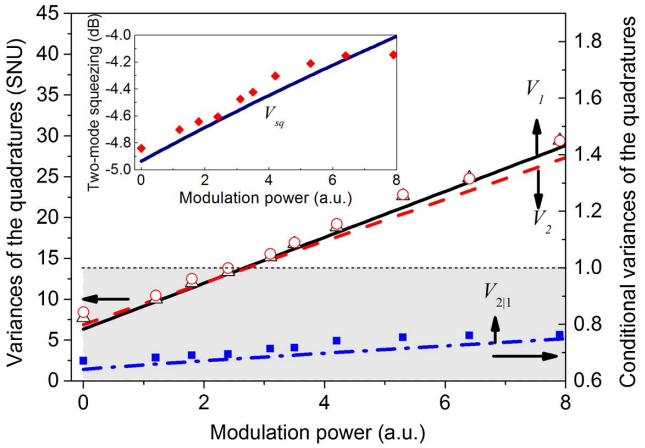

Fig. 4. Variances of phase quadratures and conditional variances of phase quadratures versus the modulation depth of the injected seed beam. The experimental points refer to V_1 (black triangles), V_2 (red circles), and $V_{2|1}$ (blue squares). Theoretical fittings: V_1 (black line), V_2 (red dashed line), and $V_{2|1}$ (blue dashed-dotted line). The shaded region denotes the presence of EPR entanglement. The inset is the two-mode squeezing vs the modulation depth.

the value of $V^X_{2|1}V^Y_{2|1}$ increases slightly to 0.54, which indicates that sufficient quantum entanglement is still maintained.

To analyze the effect of the modulation power on the quality of the quantum entanglement, the quadratures of the signal and idler fields are measured by varying the power of the electro-optic modulation of the seed field. Using the recorded quadratures, the corresponding variances, conditional variances, and two-mode squeezing are determined straightforwardly, as shown in Fig. 4. As a comparison, the theoretical predictions are also plotted using the following experimental parameters: linewidth of NOPA cavity, 17 MHz; sideband frequency, 3.5 MHz; detection efficiency of signal (idler), 0.81 (0.85); ratio of pump power and threshold power, 0.6; and escape efficiency of signal (idler), 0.86 (0.9). The experimental outcomes agree well with the theoretical predictions.

From Fig. 4, the observed variance of each EPR beam increases linearly with the modulation power, from the original case of no modulation of ∼8 to ∼30 SNUs with modulation. The conditional variance of the quadrature that indicates the EPR entanglement also increases to some extent, from 0.67 to 0.77. (The two-mode squeezing decreases accordingly.) This manifests that the EPR entanglement is degraded slightly with the increasing variances of the quadratures. This is because the modulation is applied only on the injected signal field, which results in a slight imbalance of the quadrature fluctuations between the signal and idler. This imbalance degrades the quantum correlation and, further, the EPR quantum entanglement. Note that this degradation is caused intrinsically by the imbalance of the classical modulation signal on the EPR beams, which can be recovered by adding the Gaussian modulation signal to the measured quadratures of the idler with an appropriate weight factor, i.e., $X_2 \rightarrow X_2 + gX_c$. In our experiment, the optimal value of g for recovering the initial EPR entanglement is found to be approximately −0.1.

In conclusion, we have analyzed the effects of the modulated injecting signal field on the quantum behaviors of the output fields from a NOPA. Our analysis shows that the modulation can significantly enlarge the distribution of the original EPR state in phase space, whereas it has a negligible influence on the entanglement quality. Such phenomena were also verified by the experiment. The presented scheme and device are promising candidates for quantum information processing tasks, e.g., CV QKD, in which high efficiency and a compact EPR source with signal modulation are desired. We anticipate combining the current system with the techniques of fiber devices [16] and on-chip integration [17] in the future, which will further improve the compactness and size of the current system.

Funding. National Key R&D Program of China (2016YFA0301403); National Natural Science Foundation of China (NSFC) (11774209, 61378010); Key R&D Project of Shanxi Province (201803D121065); Shanxi 1331KSC.

REFERENCES

1. H.-K. Lo, M. Curty, and K. Tamaki, Nat. Photonics **8**, 595 (2014).
2. E. Diamanti, H.-K. Lo, B. Qi, and Z. Yuan, npj Quantum Inf. **2**, 16025 (2016).
3. F. Grosshans, G. Van Assche, J. Wenger, R. Brouri, N. J. Cerf, and P. Grangier, Nature **421**, 238 (2003).
4. B. Qi, L.-L. Huang, L. Qian, and H.-K. Lo, Phys. Rev. A **76**, 052323 (2007).
5. P. Jouguet, S. Kunz-Jacques, A. Leverrier, P. Grangier, and E. Diamanti, Nat. Photonics **7**, 378 (2013).
6. S. Pirandola, C. Ottaviani, G. Spedalieri, C. Weedbrook, S. L. Braunstein, S. Lloyd, T. Gehring, C. S. Jacobsen, and U. L. Andersen, Nat. Photonics **9**, 397 (2015).
7. T. Gehring, V. Händchen, J. Duhme, F. Furrer, T. Franz, C. Pacher, R. F. Werner, and R. Schnabel, Nat. Commun. **6**, 8795 (2015).
8. N. Walk, S. Hosseini, J. Geng, O. Thearle, J. Y. Haw, S. Armstrong, S. M. Assad, J. Janousek, T. C. Ralph, T. Symul, H. M. Wiseman, and P. K. Lam, Optica **3**, 634 (2016).
9. N. Wang, S. N. Du, W. Y. Liu, X. Y. Wang, Y. M. Li, and K. C. Peng, Phys. Rev. Appl. **10**, 064028 (2018).
10. R. Garcíapatrón and N. J. Cerf, Phys. Rev. Lett. **102**, 130501 (2009).
11. V. C. Usenko and R. Filip, New J. Phys. **13**, 113007 (2011).
12. L. S. Madsen, V. C. Usenko, M. Lassen, R. Filip, and U. L. Andersen, Nat. Commun. **3**, 1083 (2012).
13. M. D. Reid, P. D. Drummond, W. P. Bowen, E. G. Cavalcanti, P. K. Lam, H. A. Bachor, U. L. Andersen, and G. Leuchs, Rev. Mod. Phys. **81**, 1727 (2009).
14. R. Horodecki, P. Horodecki, M. Horodecki, and K. Horodecki, Rev. Mod. Phys. **81**, 865 (2009).
15. X. M. Guo, C. D. Xie, and Y. M. Li, Phys. Rev. A **84**, 020301 (2011).
16. A. Brieussel, C. Fabre, K. Ott, M. Joos, and N. Treps, Opt. Lett. **43**, 1267 (2018).
17. G. Masada, K. Miyata, A. Politi, T. Hashimoto, J. L. O'Brien, and A. Furusawa, Nat. Photonics **9**, 316 (2015).